Flexible benzoxazole-containing polyimide aerogel with ultra-low dielectric constant and high dielectric strength: Synthesis and characterization

Jin-gang LIU(刘金刚)[1,3*], Xiu-min ZHANG[2], Shi-yong YANG(杨士勇)[3*]

[1] *School of Materials Science and Technology, China University of Geosciences（中国地质大学）, Beijing 100083, China;*

[2] *School of Electrical Engineering, Beijing Jiaotong University, Beijing 100044, China*

[3] *Laboratory of Advanced Polymer Materials, Inst.of Chemistry（中科院化学所）, CAS, Beijing 100190, China*

Tel: +86-10-82322104; Fax: +86-10-82322104

* *E-mail:* liujg@cugb.edu.cn; shiyang@iccas.ac.cn

In the past decades, polymer dielectrics with low dielectric constant (low-*k*) and low dissipation factor features have been paid increasing attention in ultra-large scale integrated circuit (ULSI) fabrication due to their abilities to lower the line-to-line noise in interconnects and alleviate power dissipation issues by reducing the capacitance between the interconnect conductor lines so as to achieve faster signal transmission speed [1]. Among various polymer dielectrics, polyimides (PIs) have been investigated more extensively as high performance ILDs than most other polymers due to their desirable high-temperature stability, excellent mechanical and dielectric properties for ULSI fabrications [2]. However, conventional PI dielectrics usually have *k* values around 3.0, which cannot meet the rapid development of ULSI assembly.

Very recently, aerogel dielectrics have been becoming one of the most important research topics for high performance ILDs using in ULSI due to their extremely high porosity, low density, low thermal conductivity, and ultra-low dielectric constants [3]. The porosity of an aerogel material can usually reached over 80% (volume ratio). The trapped air efficiently decreases the *k* values of the aerogels to a low level extremely closing to 1.0 for air. Among various aerogels, organic polymeric aerogels are more suitable to be used as ILDs due to their intrinsically flexible and tough nature compared with their fragile inorganic counterparts, such as silica aerogels, etc [4]. Various polymer aerogels, such as polyurethane, polyurea, polystyrene, and polydicyclopentadiene aerogels have been widely investigated in the literature and have been finding a variety of applications in high-tech fields [5]. However, common organic aerogels usually suffer from their low thermal and dimensional stability at elevated temperatures. Thus, as a representative high-temperature resistant organic aerogels, PI aerogels have been developed rapidly in recent years. For example, several PI aerogels, including aromatic multifunctional amino compound crosslinked systems [6], octa(aminophenyl)silsesquioxane (OAPS) crosslinked systems [7], amide-crosslinked systems [8], and silane-crosslinked systems [9] have been recently developed. The dielectric constants and dissipation factors for PI aerogels have also been investigated in detail. For instance, Meador and coworkers studied the dielectric properties of PI aerogels and investigated their potential applications as substrates for lightweight patch antennas for aerospace applications [10]. Relative *k* values as low as 1.16 at a frequency of X-band (~11-12 GHz) were obtained for PI aerogels made from 3,3',4,4'-biphenyltetracarboxylic dianhydride (BPDA), 2,2'-dimethylbenzidine (DMBZ), and 1,3,5-tris(4-aminophenoxy)benzene (TAB) crosslinker. Shen and coworkers have reported intrinsically highly-hydrophobic semi-alicyclic fluorinated PI aerogel with ultra-low *k* values of 1.17-1.19 in the frequency range of 2-12 GHz [11].

The dielectric constants and dissipation factor of PI aerogels have been investigated in the literature; however, the other dielectric behaviors for PI aerogels have been rarely addressed in the literature although they are also very important for their applications in ULSI. For example, in addition to low dielectric constants, the next generation of ILDs for submicron and nano-level electronics must also satisfy a variety of other requirements, including high dielectric strength and resistivity, high thermal and dimensional stability, low moisture adsorption, and good adhesion to semiconductor and metal substrates in order to achieve high reliability [12]. As we know, for porous low-*k* polymers, increasing porosity can reduce the *k* values; however, the dielectric strength is often adversely affected. To the best of our knowledge, the dielectric breakdown behavior for PI aerogels or even organic aerogels has been rarely involved in the literature.

In the current paper, as shown in **Scheme 1**, excessive 3,3',4,4'-biphenyltetracarboxylic dianhydride (BPDA) was first reacted with 5-amino-2-(4-aminophenyl)benzoxazole (APBO) to give a anhydride-capped PI precursor, poly(amic acid) (PAA) solution. Then, octa(aminophenyl)- silsesquioxane (OAPS) was added into the PAA solution inducing a crosslinking reaction of the PAA. Dehydrating agent (acetic anhydride/pyridine system) was then added into the solution affording a PI wet gel. The PI wet gel exhibited excellent flexibility and toughness, which could be bended with a large radius of curvature. Then, the PI wet gel was immersed into ethanol to extract off the NMP solvent. At last, the residual NMP and ethanol trapped in the gel was dried with $scCO_2$ at 45 °C with a pressure of 15 MPa to give the final PI aerogel (Scheme 1).

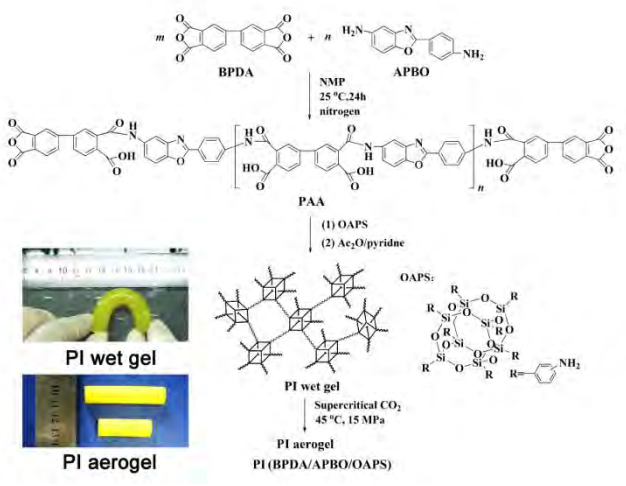

Scheme 1. Synthesis of PI (BPDA/APBO/OAPS) aerogel.

The chemical structures of the PI aerogel were identified by FT IR measurements, illustrated in **Fig. 1**. The characteristic absorption bands due to the vibration of the carbonyl groups (C=O) in the imide segments are clearly observed at 1766 cm^{-1} and 1722 cm^{-1}, which are assigned to the asymmetric and symmetric stretching vibrations, respectively. In addition, the stretching vibration of C-N bond located at 1371 cm^{-1} and the imide ring deformation at 740 cm^{-1} further confirm the formation of PI. Meanwhile, the absence of absorbing band around 1855 cm^{-1} ($\upsilon_{C=O}$ in BPDA) indicated the complete reaction of the dianhydride. Similarly, absorbing bands around 3392 cm^{-1} (υ_{N-H} in APBO) and 1640 cm^{-1}($\upsilon_{amide,\ C=O}$ in PAA) are also absent, indicating the completion reaction of the APBO and the successful conversion from the PAA precursors to PIs by chemical imidization.

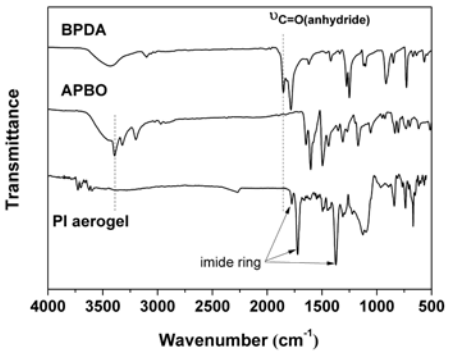

Fig. 1. FT-IR spectra of PI aerogel.

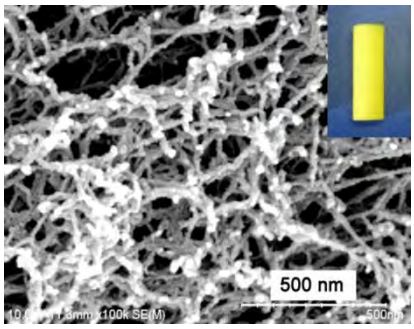

Fig. 2. SEM image of PI aerogel.

Then, the microtopography and physical parameters of the PI aerogel, including density, porosity, surface area, and volume shrinkage were investigated in detail. First, the FE-SEM measurement was performed to investigate the morphology of the PI aerogel, as shown in **Fig. 2**. For the polymer, the open-pore structure consisting of three-dimensional networks in tangled nanofibers morphology with the diameters at the nanometer scale were observed. This three-dimensional network microstructures are mainly caused by the highly crosslinking of the molecular chains in the aerogel. The solvents occupied in the networks were

continuously extracted by the solvents exchange process and following supercritical drying procedures, leaving nano pores in the final aerogels. The volume of the PI aerogel shrinks 14.5% of its original value during the supercritical drying process. This value is comparable to the PI aerogels reported in the literature [13]. The low shrinkage and microtopography for the current aerogel prove that supercritical drying is an efficient procedure producing polymer aerogels. It has been established that supercritical fluids obtained above the critical point in temperature-pressure diagram enable drying the wet polymer gels without capillary stress due to absence of liquid-vapor interfaces in the phase [14]. Using this technique, porosity higher than 85-90% and dielectric constants below 1.5 can usually be obtained.

The structural parameters for PI aerogel are tabulated in **Table 1**. The ρ_b and ρ_s values of PI aerogel were measured by mercury intrusion porosimetry method. The nanoporous structure for the aerogel endows them low bulky density (ρ_b) of 0.21 g/cm^3. Air occupies the free empty space in the aerogel with porosity of 85.6% as calculated from the ρ_b and skeletal density (ρ_s) of the aerogel. The surface areas (σ) and pore size distribution of the PI aerogel were measured by N_2 adsorption and desorption isotherms, using the Branuaer-Emmet-Teller (BET) method. As deduced from the N_2 adsorption-desorption isotherm shown in **Fig. 3**, the PI aerogel shows BET surface area of 428.6 m^2/g. The pore size distribution of PI aerogel calculated by Barret-Joyner-Halenda (BJH) method (Fig 3, insert) indicates that the average pore diameter in PI aerogel is 19.2 nm. In addition, it can be seen from **Fig. 3** that PI aerogel showed rapid increases in adsorbed volumes at relative pressure above 0.9 and the desorption plots exhibited narrow loops. All this information indicates that both mesoporous and macroporous structures exist in the PI aerogel.

Table 1. Structural parameters and thermal properties of the PI aerogel.

sample	ρ_b[a] [g/cm^3]	ρ_s[b] [g/cm^3]	porosity [c] [%]	σ [d] [m^2/g]	d [e] [nm]	$T_{5\%}$[f] [^{o}C]	R_{w750}[g] [%]	T_g[h] [^{o}C]
PI aerogel	0.21	1.46	85.6	428.6	19.2	502	66.7	358.3

[a] Bulk density. [b] Skeletal density. [c] Calculated by 1-(ρ_b/ρ_s). [d] Brunauer-Emmett-Teller (BET) surface area. [e] Average pore diameter from the BJH desorption plot. [f] Temperature at 5% weight loss. [g] Residual weight ratio at 750 oC in nitrogen. [h] Glass transition temperature.

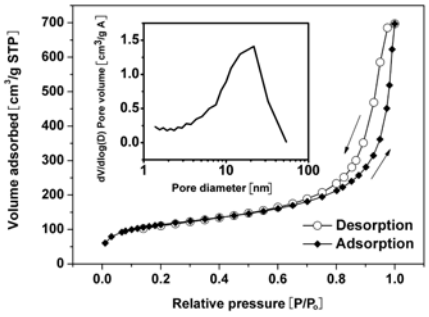

Fig. 3. N_2 adsorption-desorption isotherm data for PI aerogel.
(Insert: pore size distribution plot).

Thermal properties of the PI aerogel were evaluated by thermogravimetric analyses (TGA) and thermalmechanical analyses (TMA) measurements and the data were tabulated in Table 1. The TGA measurements of the PI aerogels were performed in nitrogen from 50 ^{o}C to 750 ^{o}C and the results are shown in **Fig. 4**. From the plot, it can be observed that the aerogel showed good thermal stability up to 450 ^{o}C. The smooth plots around 300 ^{o}C indicated the complete remove of residual NMP solvent by the supercritical drying procedure and the complete imidization in the system. The 5% weight loss temperatures ($T_{5\%}$) are 505 ^{o}C and the residual weight ratio (char yield) of the aerogel at 750 ^{o}C is 66.7% in nitrogen, indicating good thermal stability of the aerogel.

The dimension changes of aerogel at elevated temperatures are investigated by TMA measurements, as depicted in **Fig. 5**. The aerogel showed expansion behavior after the occurrence of glass transition around 350 ^{o}C. A T_g value was recorded at 358.3 ^{o}C for the aerogel. This value is much high than those of common polymer aerogels, which can guarantee the good reliability of the aerogel in ULSI fabrication.

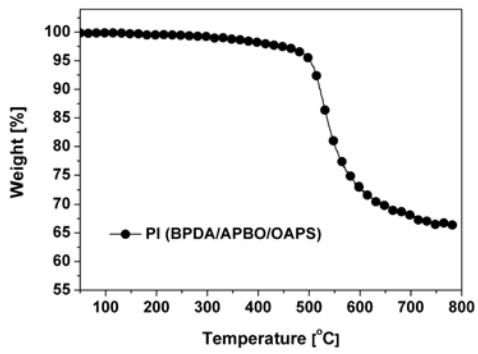

Fig. 4. TGA plot of PI aerogel.

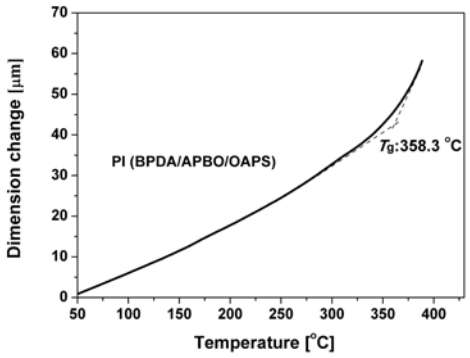

Fig. 5. TMA plot of PI aerogel.

The dielectric properties of the PI aerogel, including surface (ρ_S) and volume (ρ_V) resistivity, dielectric strength, dielectric constant and dissipation factor were investigated. These dielectric parameters are critical for their applications in ULSI applications. As shown in **Table 2**, the ρ_V and ρ_S values for the aerogel are 5.45×10^{16} Ω·cm and 8.74×10^{14} Ω, respectively, indicating excellent electrical insulation properties. The dielectric breakdown strength of the aerogel is 132 kV/cm at a thickness of 2.5 mm in our measurement. This value is a bit higher than expected for porous materials. Similar phenomenon has also been observed by Hrubesh and coworkers in their research on inorganic silica aerogels [15]. In their investigation, the dielectric strength of 128 kV/cm was recorded for silica aerogels and this value was higher than those of common ceramics, such as alumina (110 kV/cm) although lower than those of pure polymers (160-500 kV/cm). The authors ascribed this unexpected high dielectric strength for aerogels to the small pore sizes in the air-filled aerogels. The pore sizes are of the same order as the mean free path for electron collisions. Thus, electrons in aerogel pores tend to collide with the solid before gaining sufficient kinetic energy to ionize upon impact. In the current work, the dielectric strength of 132 kV/cm at a thickness of 2.5 mm was recorded, which is comparable to that of inorganic silica aerogels.

Table 2. Dielectric properties of the PI aerogel.

	ρ_V [a]/[Ω·cm]	ρ_S [a]/ [Ω]	d [b] [mm]	D_S [c] [kV/cm]	k [d]	δ [e]
PI aerogel	5.45×10^{14}	8.74×10^{13}	2.5	132	1.15	0.0023

[a] ρ_V and ρ_S: volume and surface resistivity at 23°C and 50% relative humidity, respectively; [b] PI aerogel thickness for k measurements; [c] dielectric breakdown strength; [d] dielectric constant at 2.75 GHz; [e] dielectric loss factor at 2.75 GHz.

We further investigated the dielectric breakdown behavior for the PI aerogel. **Fig. 6** compares the surface macro- and micro-topographies of PI aerogel before and after dielectric breakdown under high voltage. From the illustration, we can obviously observe that high level electrical voltage induces not only the dielectric breakdown, but apparent surface ablation phenomena in the tested area. Many pinholes were observed at the tested area, indicating dielectric breakdown of the PI solid. Basically, the dielectric properties of aerogels are dominated by the large volume fraction of trapped gas in the pores. However, during our measurement for dielectric breakdown, bright spark was observed at the moment of electrical breakdown, indicating a gaseous discharge. Meanwhile, high voltage breakdown occurred in the dense PI solid. Thus, the dielectric breakdown for PI aerogel might be ascribed to the simultaneous actions of high voltage to the trapped air and the dense PI solid. High temperature induced by the air discharge caused the surface ablation of the aerogel. At the same time, the instantaneous high temperature caused the expansion of the trapped air in the aerogel, resulting in the swelling at the surface of the aerogel (picture b in Figure 7). Nevertheless, the high dielectric breakdown strength makes the current PI aerogel to be effective and lightweight dielectric insulators for high-voltage insulating applications.

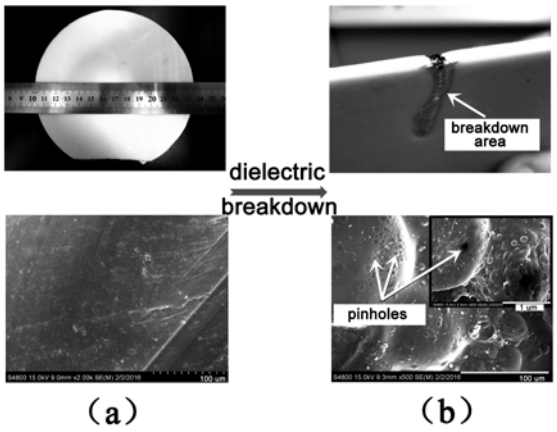

Fig. 6. Surface topographies of PI aerogel before (a) and after (b) dielectric breakdown.

The broadband dielectric constant (k) and dissipation factor (δ) of PI aerogel in the frequency range of 2-12 GHz were measured at room temperature and the curve is illustrated in **Fig. 7**. The monolithic PI aerogel sample (50 mm ×30 mm×2.5 mm) exhibited nearly a constant k value (1.15-1.13) over the entire frequency range. Thus, introduction of air within the PI reduced the k value significantly. The loss tangent (δ) value of PI aerogel also changed in a narrow range of 2.3×10^{-3}-4.0×10^{-3}. The frequency-independent feature of k and δ values for PI aerogel is mainly attributed to the high air loading (porosity: 85.6%) in its structure. The phenomena indicate that the dielectric constant of the PI aerogel is dominated by the trapped air rather than by the solid PI matrix.

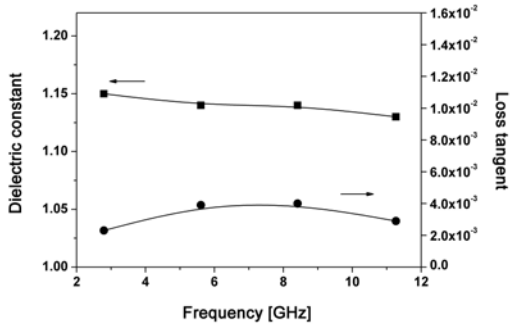

Fig. 7. Dielectric constant (k) and loss tangent for PIA as a function of frequency.

In summary, new PI aerogel was synthesized from BPDA, APBO and OAPS via two-step chemical imidization procedure, followed by $ScCO_2$ drying procedure. The original purpose of molecular design aiming at developing functional PIs with potential applications as ILDs for ULSI was successfully achieved by the derived PI aerogel. The polymer exhibited excellent thermal stability and T_g over 350 °C. They have excellent dielectric characteristics, including ultra-low k value and dissipation factor over a broad frequency range of 2-12 GHz, high surface and volume resistivity, and high dielectric strength. The k value around 1.15 at a frequency of 2.75 GHz is one the lowest values for PI materials reported in the literature. Thus, good combined properties make the PI aerogel a good candidate as interlayer dielectric for advanced semiconductor chip interconnection.

Acknowledgements

Financial support from the National Basic Research Program (973 Program) of China (2014CB643605), and Fundamental Research Funds for the Central Universities are gratefully acknowledged.

References

[15] Volksen W., Miller R-D., Dubois G. Chemical Reviews, **110**, 56-110 (2010).

[16] Liaw D-J., Wang K-L., Huang Y-C., Lee K-R., Lai J-Y., Ha S-K. Progress in Polymer Science, 37, 907-974 (2012).

(more reference goto p52)